2024 IEEE International Conference on Robotics and Automation (ICRA 2024)
May 13-17, 2024. Yokohama, Japan

Hybrid Robot for Percutaneous Needle Intervention Procedures: Mechanism Design and Experiment Verification

Hanyi Zhang[1], Guocai Yao[1], Feifan Zhang[2], Fanchuan Lin[3] and Fuchun Sun[1]

***Abstract*— This paper presents a 6-DOF hybrid robot for percutaneous needle intervention procedures. The new robot combines the advantages of both serial robots and parallel robots, featuring compactness, high accuracy, and small footprint while overcoming the problems of the high cost of serial robots and the small workspace and singularity issue of parallel robots. Besides, by analyzing the workspace of the robot, the equation is derived between the structure parameter and workspace to adjust the parameters of the robot to satisfy different working scenes. According to the experiment, the accuracy of the robot is related to the position, distance, and insertion angle. The result shows that the performance is better when working near the center workspace and away from the servos and the average error of the robot is 1.39mm. The phantom experiment of lumbar puncture validates its feasibility.**

I. INTRODUCTION

Percutaneous interventions are significant minimally invasive clinical procedures mainly applied in diagnostic and therapeutic, such as biopsies[1], abscess drainages, tumor ablations[2, 3], and drug administration, involving many anatomical sites[2, 4], including breast[5, 6], brain[7], prostate[8-11], bones[12-14], and internal organs[3, 15]. Positioning is a critical but challenging task in percutaneous interventions. However, it is very difficult to achieve needle insertion precision within 3mm[16] by positioning manually, and CT guidance typically achieves an accuracy of around 5mm[17] due to the limitation of human hands and it highly relies on the experience of surgeons. Besides, to position the target, many procedures are guided by images, which makes doctors exposed to X-rays. The medical robot can not only improve the position accuracy but also have the potential to avoid radiation damage to doctors[18, 19].

The existing robots for percutaneous interventions can be divided into two categories: serial robots and parallel robots. The serial robot arm is the most common type applied in many situations due to its early development[20, 21]. The ROSA robot[22, 23] from Zimmer Biomet, UK, is one of the most widely used medical robots including the ROSA One Brain, ROSA Knee, and ROSA One Spine which are used for minimally invasive surgery related to the brain, knee, and spine, respectively. Zimmer Biomet has chosen to design its robotic platform with an industrial 6 degrees of freedom (DOF) robotic arm and the accuracy can be achieved within 1mm. However, the accuracy of the robot comes at a cost and in a large size. Serial robots consist of several active joints connecting the end effector and the base, which feature high dexterity and large workspace but suffer from low precision, large footprint, and high cost[24].

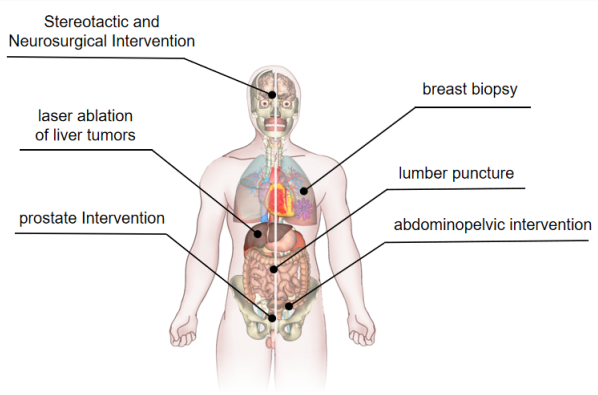

Fig. 1. The wide range of applications of percutaneous intervention robotic systems.

Parallel robots developed much later than serial robots. Maurin et al.[25] present a parallel robot named CT-Bot composed of a needle driver and a positioner. CT-Bot has 5 DOF: 3 DOF for the position and 2 DOF for the orientation. Plitea et al.[26] present a new 5-DOF modular parallel robotic structure for brachytherapy. The new structure has a small occupied volume and can be compatible with the CT scanners used in the procedures, which will enhance the accuracy of the needle positioning and seed delivery, reducing radiation exposure. Parallel robots consist of at least two independent kinematic chains connecting the moving platform and the fixed platform, which feature high precision and velocity but suffer from low dexterity and small workspace. The conflict of high precision and large workspace has been a constant challenge for positioning robots, especially for systems that require high speed and muti-DOF.

To solve this issue, hybrid robots based on parallel mechanisms have been proposed to be applied in the percutaneous needle intervention procedure. Patel et al.[13] developed a body-mounted 4-DOF mechanism robot for percutaneous interventions. Salimi et al.[27] designed a 4-DOF MRI-compatible and cable-driven manipulator called ROBOCATH

[1]Hanyi Zhang, Guocai Yao, Fuchun Sun are with Department of Computer Science and Technology, Tsinghua University, Beijing, 100084, China h.zhang23@imperial.ac.uk [yaoguocai,fcsun]@tsinghua.edu.cn
[2]Feifan Zhang is with the Department of Computer Science, University College London, WC1E 6BT, London, UK feifan.zhang.22@ucl.ac.uk
[3]Fanchuan Lin is with the Department of School of Instrumentation and Optoelectronic Engineering, Beihang University, Beijing, 100191, China Linffcc@buaa.edu.cn

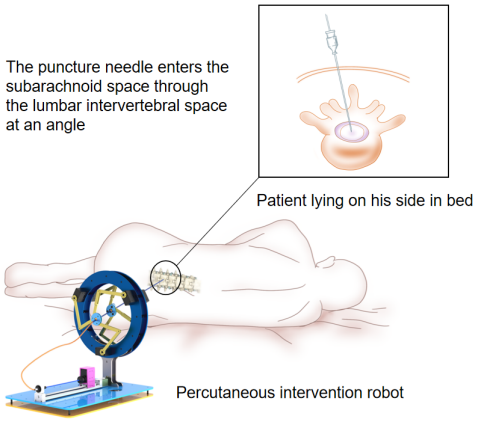

Fig. 2. The working process of the percutaneous intervention robot with the example of lumbar puncture.

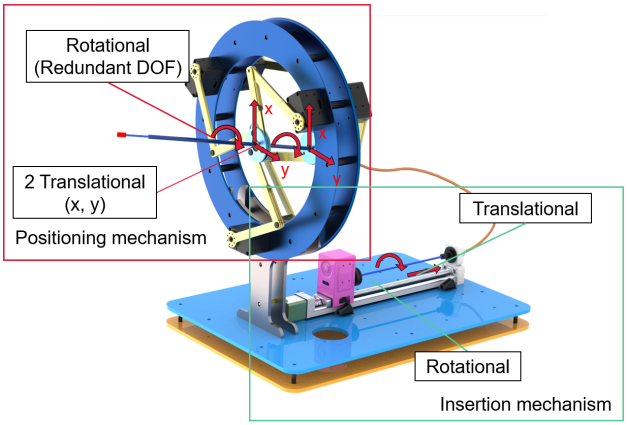

Fig. 3. The robot provides 6 DOF: each layer of the positioning mechanism has 2-DOF for localization of the moving platform on the plane with 1 redundant DOF to improve the performance and the insertion mechanism has 2-DOF (one for insertion, another for needle rotation).

in transapical beating-heart interventions. Both of them consist of two layers of planers to adjust the direction and position of the needle. However, They all involve the rotation of the planer which leads to low movement efficiency and the complex control system. Therefore, the development of a robot with excellent comprehensive performance is significant for positioning issues.

This paper proposes a hybrid robot that combines the advantages of both serial and parallel robots and features small volumetric and compactness. This robot is based on two 3-RRR parallel mechanisms, thus featuring high precision and speed as parallel robots. Compared to the previous hybrid robots involving the rotation of planers, the 3-RRR mechanism also makes it easy to control and move with high efficiency. Two 3-RRR parallel mechanisms are connected in series, which enlarges its workspace and enhances its dexterity, leading to the advantages of serial robots.

II. ROBOT DESIGN AND KINEMATIC MODELLING

A. Robot design

As shown in Fig. 2, percutaneous interventions require the needle to be inserted into a target along a certain direction, thus demanding the robot to have the ability to position and insert. The hybrid robot in this paper has 6 degrees of freedom and consists of two modules: the positioning mechanism and the needle insertion mechanism, which are independent of each other. The positioning mechanism consists of two layers of planar positioning mechanism. The upper platform and the lower platform adopt the same structure and are parallel to each other and co-axial, each providing 3-DOF motion (two for the x, and y coordinates, one for rotation around the z axis) respectively. With the coordinates of two points on different planes determined, the direction and position of the needle guide are determined. Some research has shown that rotating a bevel needle at a proper speed while inserting can reduce the displacement from the target[15, 28-30] thus demanding the robot to have the ability to rotate the needle, which is rarely considered in previous research. Therefore, the needle insertion mechanism has 2-DOF, which is used to advance the needle forward and rotate it. Fig. 3 shows the fully assembled robot and the two modules.

The positioning module consists of two layers of 3-RRR planar parallel manipulator which features high accuracy, simple structure, and high movement efficiency. Each layer is driven by three servos (XM430-W350, Robotis, Korea) on the static platform, to determine the position of the moving platform in the plane and the rotation angle. A spherical hinge is embedded in the moving platform for connecting the puncture needle guide, so that the needle insertion mechanism will not rotate with the platform rotation, thus converting the rotational degrees of freedom of the 3-RRR manipulator into redundant degrees of freedom, which is used to avoid the singularities and improve the dexterity of the mechanism in order to optimize the performance of the mechanism. As shown in Fig. 4 (a), the upper platform ball hinge and the catheter adopt interference fit to fix the needle guide, and the lower platform adopts gap fit to connect with the needle guide, so as to adapt to the change of its length between the two platforms when the needle guide changes its attitude. As shown in Fig. 4 (b), the needle insertion module is a concentric tube robot. A Ni-Ti alloy wire is inside the hollow tube and a needle can be fixed on the end of the wire. With the direction of the needle determined by the needle guide tube, the screw drives the needle to advance, and the servo controls the rotation of the needle.

The hybrid robot not only meets the requirement of most percutaneous intervention procedures but also combines the advantages of both serial and parallel medical robots, featuring high accuracy, compactness, and small footprint. Besides, compared to the existing robots, the rotational DOF of the needle insertion mechanism gives it the potential to achieve higher accuracy in vivo.

B. Kinematic modeling

Kinematic modeling is the basis for parameter optimization and the robot control system. In this section, we first

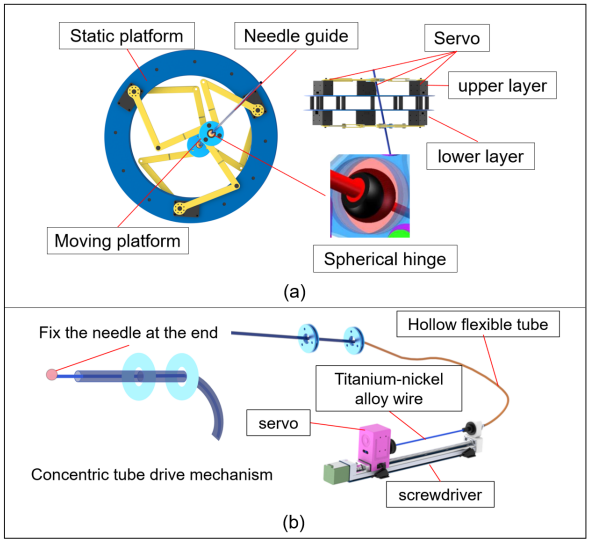

Fig. 4. The assembly rendering of two modules. (a) The positioning module is composed of double 3-RRR parallel planar manipulators and uses the spherical hinge to fix the needle guide. Each layer is driven by three servos. (b) The needle insertion module is a concentric tube robot. A flexible but hard NiTi alloy wire inside the tube is driven by a screwdriver to advance and a servo to rotate.

consider the inverse kinematic modeling between the needle tip and two planar manipulators and then develop the inverse kinematic equation of the individual 3-RRR planar parallel manipulator, so as to obtain the inverse kinematic model of the whole robot. The forward kinematics needs to be solved by the numerical iteration method, which is computationally intensive and costly in terms of computational time, and the positive kinematics model is not applicable to the analysis of this structure[31]. Therefore, we just discuss and build the inverse kinematic modeling in this section.

1) kinematic model between the needle and the dual platform of the positioning module. As shown in Fig. 5, The z-coordinate of plane1 is 0 and the spacing between the two platforms is D. The end effector of plane1 coordinate is $O_1(x_1, y_1, 0)$, and the end effector of plane2 coordinate is $O_2(x_2, y_2, D)$.

The target point position is defined $P(x_0, y_0, z_0)$, and the vector $\vec{p}(x_d, y_d, z_d)$defines its direction.

$$\frac{x_1 - x_0}{x_d} = \frac{y_1 - y_0}{y_d} = \frac{0 - z_0}{z_d} \tag{1}$$

$$\frac{x_2 - x_0}{x_d} = \frac{y_2 - y_0}{y_d} = \frac{D - z_0}{z_d} \tag{2}$$

From Equations (1) and (2), the O_1, O_2 can be expressed as follow:

$$O_1 = \begin{pmatrix} x_1 \\ y_1 \\ 0 \end{pmatrix} = \begin{pmatrix} \frac{-z_0}{z_d} x_d + x_0 \\ \frac{-z_0}{z_d} y_d + y_0 \\ 0 \end{pmatrix} \tag{3}$$

$$O_2 = \begin{pmatrix} x_2 \\ y_2 \\ 0 \end{pmatrix} = \begin{pmatrix} \frac{D - z_0}{z_d} x_d + x_0 \\ \frac{D - z_0}{z_d} y_d + y_0 \\ D \end{pmatrix} \tag{4}$$

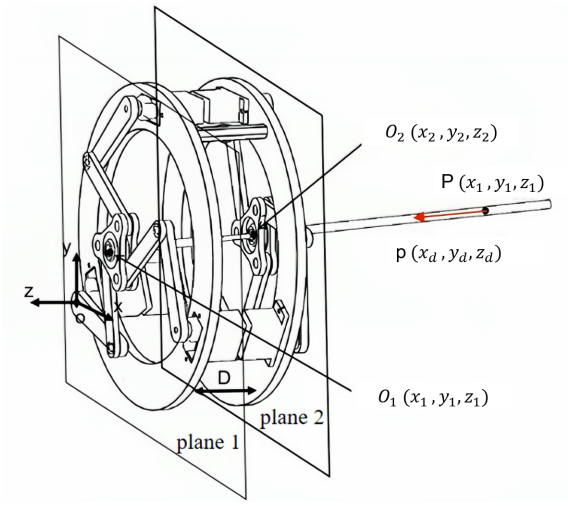

Fig. 5. The assembly rendering of two modules.

2) kinematic model of the single parallel planar manipulator. The inverse kinematics of the 3-RRR planar parallel mechanism is solved to establish the equation between the pose of the end-effector and the angles of servos. Combining with the kinematics equation between needle and positioning modules obtained above, the overall inverse kinematics solution for this robot can be derived. s shown in Fig. 6, R is the radius of the static platform $A_1A_2A_3$, r is the radius of the moving platform $C_1C_2C_3$. The coordinates of the servos joints are:

$$A = \begin{bmatrix} A_1 & A_2 & A_3 \end{bmatrix} = \begin{bmatrix} 0 & \sqrt{3}R & \frac{\sqrt{3}}{2}R \\ 0 & 0 & \frac{3}{2}R \end{bmatrix} \tag{5}$$

The coordinates of the servos joints with respect to the centre M are:

$$C^M = \begin{bmatrix} C_1^M & C_2^M & C_3^M \end{bmatrix} = \begin{bmatrix} -\frac{\sqrt{3}}{2}r & \frac{\sqrt{3}}{2}r & 0 \\ -\frac{1}{2}r & -\frac{1}{2}r & r \end{bmatrix} \tag{6}$$

The spatial transformation matrix T for transforming frame M into frame N is shown as follows:

$${}^M_N T = \begin{bmatrix} \cos\alpha & -\sin\alpha & 0 & x \\ \sin\alpha & \cos\alpha & 0 & y \\ 0 & 0 & 1 & 0 \\ 0 & 0 & 0 & 1 \end{bmatrix} \tag{7}$$

The coordinates of the moving platform center in the static coordinate system can be expressed as follows:

$$\begin{bmatrix} C_i \\ 1 \end{bmatrix} = {}^M_N T \begin{bmatrix} C_i^M \\ 1 \end{bmatrix} \tag{8}$$

From equations(7) and (8), C can be expressed as follows:

$$\begin{bmatrix} C_1 & C_2 & C_3 \end{bmatrix} = \begin{bmatrix} x - r\cos\left(\frac{\pi}{6} + \alpha\right) & x + r\cos\left(\frac{\pi}{6} - \alpha\right) & x - r\sin\alpha \\ y - r\sin\left(\frac{\pi}{6} + \alpha\right) & y - r\sin\left(\frac{\pi}{6} - \alpha\right) & y + r\cos\alpha \end{bmatrix} \tag{9}$$

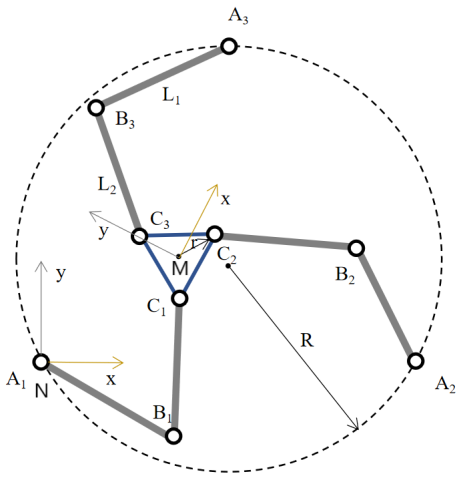

Fig. 6. Schematic diagram of 3-RRR parallel planar manipulator and kinematic parameters.

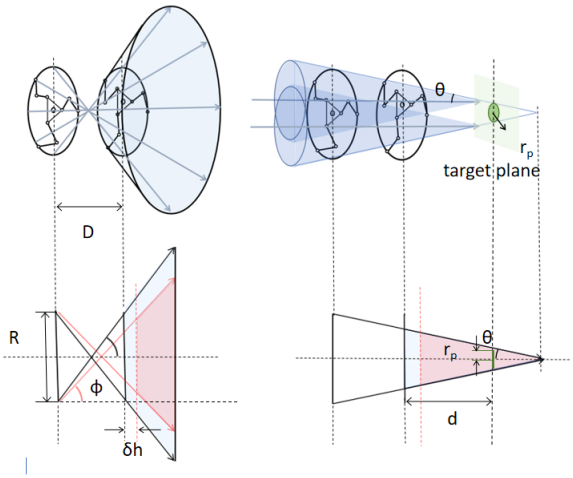

Fig. 7. The left is the reachable workspace for locating-only work and the right one is the workspace for work with requirements of both location and orientation. For the diagram of the second row, the blue scale is the ideal workspace and the red scale is the actual workspace with introducing modified parameter.

For each branch $A_iB_iC_i$, it satisfies the following vector equation:

$$\overrightarrow{N_iC_i} = \overrightarrow{N_iA_i} + \overrightarrow{A_iB_i} + \overrightarrow{B_iC_i} \tag{10}$$

After solving Equation (10), the input variable of the robot can be expressed as follows:

$$\theta_i = 2\arctan\left(\frac{-k_{i1} \pm \sqrt{k_{iws}}}{k_{i3} - k_{i2}}\right) \tag{11}$$

where

$$\begin{gathered} k_{iws} = k_{i1}^2 + k_{i2}^2 - k_{i3}^2 \\ k_{i1} = 2L_1\left(y_{Ai} - y_{Ci}\right) \\ k_{I2} = 2L_1\left(x_{Ai} - x_{Ci}\right) \\ k_{i3} = x_{Ci}^2 + y_{Ci}^2 + x_{Ai}^2 + y_{Ai}^2 - 2x_{Ci}x_{Ai} - 2y_{Ci}y_{Ai} + l_1^2 - l_2^2 \end{gathered}$$

From equation (12), each branched chain has two solutions, therefore, there are eight configurations of 3-RRR planar parallel manipulator. Kock et al.[32] carried out a comparative study on the performance of several configurations, and the results showed that the performance of 3-RRR in symmetric configuration is more symmetric and centralized, with a better performance in the central region.

III. WORKSPACE ANALYSIS AND STRUCTURE PARAMETER DESIGN

The reachable workspace of the robot can be solved in the geometric method. The reachable workspace can be obtained through the limit positions in the two 3-RRR parallel manipulators as Fig. 7 shown. In the ideal case, the height of this frustum h of the cone is determined by the needle insertion mechanism and the angle of generatrix is $arctan(2R/D)$, where R is the radius of the workspace of the planar parallel manipulators and D is the spacing between the two manipulators. In the actual case, limited by the actual mechanical structure, the needle feed angle may not reach $arctan(2R/D)$, and hard to work close to the manipulators. The maximum reachable angle ϕ and the correction height δh can be introduced to modify it.

The reachable workspace obtained by the above method is more suitable for simple point positioning task which has no requirement for the angle, but in some puncture procedures, there is often a certain requirement for the angle of the needle insertion. Let the maximum angle required for the needle feed be θ, the workspace is a cone with $R - Dtan\theta$ as the radius of the bottom surface and $R/tan\theta - D$ as the height as shown in Fig. 7. Besides, the maximum reachable angle should be guaranteed greater than θ under interference in the manufacturing process.

Based on the workspace analysis above, the structure's parallel can be designed according to requirements of the actual work. Take the following situation as an example: the targets are on the plane which is d away from the robot and the distance between the farthest target and the central point is r_P. According to the analysis, the structure parameters of the robot should satisfy the equation:

$$(R/tan\theta - D - d)tan\theta > r_p \tag{12}$$

IV. EXPERIMENT AND RESULTS

A. Accuracy assessment and analysis

To characterize the accuracy of the needle positioning module, we chose a laser transmitter with a diameter of 6mm to be fixed on the end of the actuator, and a laser receiver plate on the opposite side to the mechanism, which identifies the position of the laser spot center by means of a binocular camera. The target position is transmitted to the positioning mechanism via the computer, which makes the end-effector move to the corresponding position, making the laser spot center move to the target. The setup of the experiment is shown in Fig. 8. Before the experiment starts, the origin of the coordinates needs to be calibrated: the coordinates

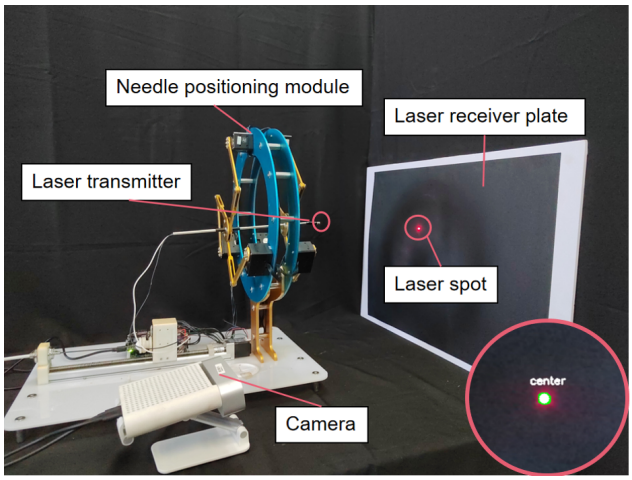

Fig. 8. Experiment setup: the robot, camera, laser transmitter, laser receiver plate. The recognition result of the laser spot on the image from the camera by the computer is shown in the red circle at the lower right corner. The recognition algorithm performs well.

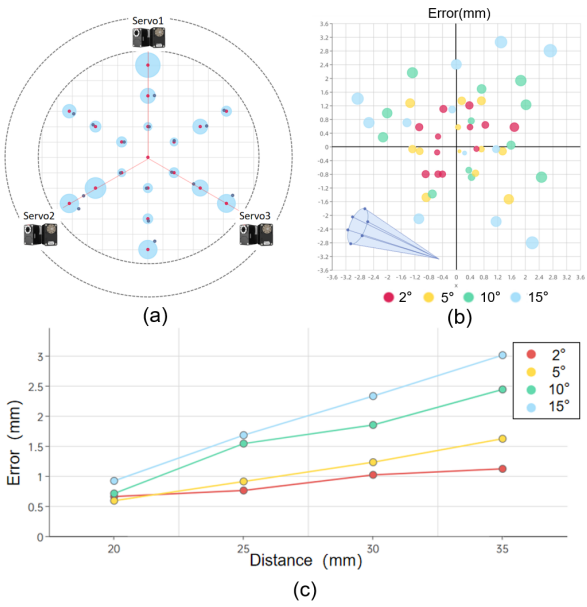

Fig. 9. (a) The locations of the targets and corresponding actual spots on the plate obtained in the experiment: The red spots are the desired targets and the blue spots are the actual laser spots. The area of blue bubbles represents the error at each target. The result of lasing to different positions vertically shows that the error is positively correlated with the distance from the center and the error is larger in the groups whose target is close to servos. (b) The position of the bubbles of different colors shows the locations of the actual laser spots obtained by lasing at different angles and the area of bubbles represents the error. For the experiment of each angle, six directions are set as the the lower left diagram shown. (c) The errors of lasing to the same location at different angles and distances.

$O(0,0)$ are transmitted to the mechanism, making the laser point move to the origin. Then the original coordinates of the point in the camera are acquired in the camera. Repeat the process ten times and take the average of the horizontal and vertical coordinates to define this position as the origin of the coordinate system in the camera.

To characterize the accuracy of the positioning mechanism locating targets in different positions, the targets are set on circles with a radius of 10mm, 20mm, and 30mm respectively with the distance between the receiver panel and the robot being set to 300mm. On each circle, the targets are set in six uniform locations within the robot's workspace according to the symmetry of the robot. Using the targets' x-y location as the input to the mechanism and setting the insertion angle of the needle to 0 degrees, the laser transmitter was placed in the corresponding position to lase to the target location on the receiver plate. The actual position of the center of the laser points is obtained by the camera to calculate the error between the target position and the actual position. The experimental results show that the average error of the mechanism at 10mm, 20mm, and 30mm away from the center is 0.59mm, 1.67mm, and 2.46mm, and the average error of different locations is 1.38mm. As shown in Fig. 9 (a), it can be concluded that the closer the positioning mechanism is to the center, the better the accuracy performance. Besides, the accuracy is higher at the position away from the servos than near the servos (along the red line in Fig. 9 (a)). The result is consistent with the performance distribution characteristics of the 3-RRR mechanis[33] which is the main reason for the distribution of the error.

To characterize the accuracy of the positioning mechanism locating in the same target locations at different angles, set the distance between the receiver panel and the robot to 300mm, the laser was demanded to reach the origin of the coordinates at an angle of 2 degrees, 5 degrees,10 degrees, and 15 degrees. According to the symmetry of the robot, in each group, we set six directions in the cone as shown in Fig. 9 (b) to reach the target point at the same angle. The experimental results show that the average error of the mechanism with the angle of 2 degrees, 5 degrees, 10 degrees, and 15 degrees is 1.00mm, 1.23mm, 1.84mm, and 2.33mm, and the average error of different locations is 1.60mm. The process was repeated the two times to get the average values. As shown in Fig. 9 (b), it can be concluded that the larger the insertion angle is, the worse the accuracy is. In this experiment, the different angles were achieved by changing the position of the moving platforms of two 3-RRR planers. The error increases with the increasing of the distance between moving platforms and the center of planers.

To characterize the accuracy of the positioning mechanism locating the targets at different distances, the laser receiver plate is placed at distance of 200mm, 250mm, 300mm, and 350mm for the mechanism to reach the targets $(0,0)$ at different distances. In each group, the mechanism lases to the target at six different angles and the experimental results are shown in Fig. 9 (c). The experimental results show that the average error of the mechanism at the distances of 200mm, 250mm, 300mm, and 350mm is 0.72mm, 1.22mm, 1.61mm, and 2.04mm, and the average error of different locations is 1.39mm. As shown in Fig. 9 (c), the shorter the distance, the higher the accuracy. Besides, with the increase of the

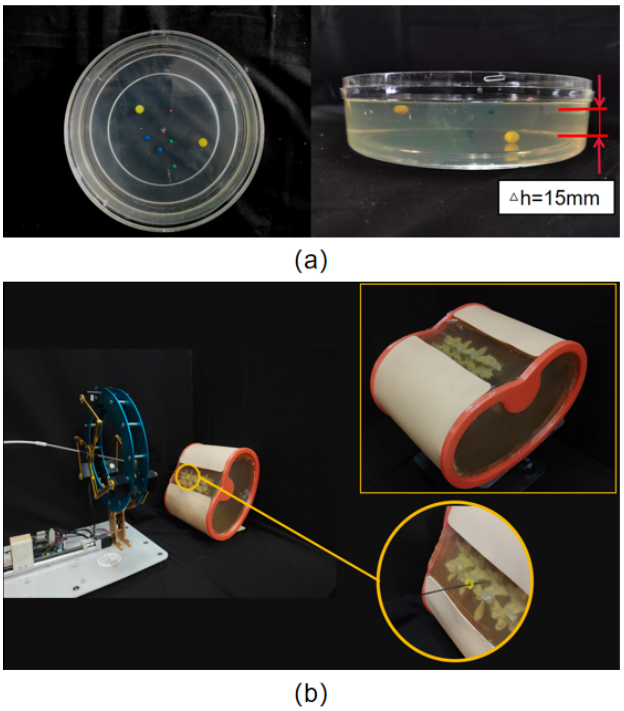

Fig. 10. (a) The accuracy validation experiment within gelatin: Beads of different colors are with different Diameters: yellow: 8mm, blue: 5mm, green: 3mm, red: 2mm. The distance between two layers is 15mm. (b) The lumbar phantom and feasibility evaluation experiments.

distance, the change of the error brought about by the change of angle increases, which means the error is more sensitive to the change of angle.

TABLE I
RESULT OF THE ACCURACY EXPERIMENT

Accuracy at different distances from the center of the mechanism					
distance(mm)	10	20	30	-	mean
error(mm)	0.59	1.67	2.46	-	1.38
Accuracy at different angle					
angle(°)	2	5	10	15	mean
error(mm)	1.00	1.23	1.84	2.33	1.60
Accuracy at different distances from the receiver panel					
distance(mm)	200	250	300	350	mean
error(mm)	0.72	1.22	1.61	2.04	1.39

B. Lumbar puncture validation

In order to test the feasibility of the mechanism in percutaneous interventions, a stiff needle was mounted on the end of the actuator to simulate the insertion of a puncture needle, and different body model experiments were designed to validate the mechanism using gelatin instead of human tissue. In order to validate the robot's localization mechanism for different target sizes at different depths and locations, a gelatine model as in Fig. 10 (a) was designed: the target was placed in different depths of gelatine and different target sizes were placed in each layer. the larger beads stand for more feasible clinical targets while the smaller beads stand for more challenging targets. In this experiment, the needle needs to reach each target through the alimentary gelatin. The result shows that all the targets can be reached accurately in the alimentary gelatin, validating the accuracy of the robot working in the phantom.

The phantom is constructed according to the sizes of the human body to simulate the human waist as shown in Fig. 10 (b) the phantom was sealed all around with a Lumbar spine model embedded in the inside gelatin and a view window was on the front, back and top. According to the previous research on lumbar puncture, the body landmark for puncture the L4 spinous process located at the intersection of Tuffier's line and the lumbar spine midline, and the diagnostic Lumbar Puncture should be performed at the L3/4 interspinal space[34, 35]. Therefore, a hole was drilled at the same location on the top of our phantom and the needle needs to through the hole to obtain CSF samples after piercing the ligamentum flavum, dura, arachnoid, etc. The experiment results show that the robot can successfully insert into the spine to reach the target location through the hole.

V. CONCLUSION AND FUTURE WORK

In this paper, we describe a hybrid robot for percutaneous interventions and validate its performance. This hybrid robot features high accuracy, small footprint, compactness, and enough workspace by combining the advantages of both serial robots and parallel robots. The compactness and small size make it possible to work in the MRI scanner, whose bore size (600-700mm) hinders applications of both doctors and numerous serial robots, and to be fixed on other robots ends to obtain larger workspace with high accuracy, thus giving it potential for a wide range of applications. Moreover, the redundant degree of freedom makes it avoid the singularity successfully, which overcomes a big problem for the parallel manipulator. The innovative needle insertion mechanism can support it to reach a higher accuracy by avoiding deviation caused by human tissue due to the design of the rotational DOF of the needle. This paper also proposes the method and equations to adjust the structure parameters of the robot to satisfy the different requirements of the workspace according to the calculation and analysis of the workspace. In the experiment, the accuracy can reach a submillimeter scale when working near the center part of the robots. Positioning to different locations at different directions and distances, the accuracy is much less than 5mm. The experiment result shows that the accuracy of the robot can satisfy the requirement of most kinds of percutaneous needle interventions and validates its feasibility by working with a phantom.

In the future, to achieve higher accuracy and repeatability, the design of some fastenings of the mechanism needs to be improved and the error compensation experiments and calculations need to be conducted. Besides, in order to realize MRI compatibility, actuators with electromagnetic compatibility needed to be found or designed to replace the traditional servos.

REFERENCES

[1] R. Mieling et al., "Collaborative Robotic Biopsy with Trajectory Guidance and Needle Tip Force Feedback," in 2023 IEEE International

Conference on Robotics and Automation (ICRA), 2023, pp. 6893-6900.
[2] M. J. Musa, K. Sharma, K. Cleary, and Y. Chen, "Respiratory compensated robot for liver cancer treatment: Design, fabrication, and benchtop characterization," IEEE/ASME Transactions on Mechatronics, vol. 27, no. 1, pp. 268-279, 2021.
[3] E. Franco, D. Brujic, M. Rea, W. M. Gedroyc, and M. Ristic, "Needle-guiding robot for laser ablation of liver tumors under MRI guidance," IEEE/ASME Transactions on Mechatronics, vol. 21, no. 2, pp. 931-944, 2015.
[4] P. Kulkarni, S. Sikander, P. Biswas, S. Frawley, and S.-E. Song, "Review of robotic needle guide systems for percutaneous intervention," Annals of biomedical engineering, vol. 47, pp. 2489-2513, 2019.
[5] D. Navarro-Alarcon et al., "Developing a compact robotic needle driver for MRI-guided breast biopsy in tight environments," IEEE Robotics and Automation Letters, vol. 2, no. 3, pp. 1648-1655, 2017.
[6] B. Yang, U.-X. Tan, A. B. McMillan, R. Gullapalli, and J. P. Desai, "Design and control of a 1-DOF MRI-compatible pneumatically actuated robot with long transmission lines," IEEE/ASME transactions on mechatronics, vol. 16, no. 6, pp. 1040-1048, 2010.
[7] C. He, R. H. Nguyen, C. Forbrigger, J. Drake, T. Looi, and E. Diller, "A Hybrid Steerable Robot with Magnetic Wrist for Minimally Invasive Epilepsy Surgery," in 2023 IEEE International Conference on Robotics and Automation (ICRA), 2023, pp. 6830-6836.
[8] A. Krieger et al., "Development and evaluation of an actuated MRI-compatible robotic system for MRI-guided prostate intervention," IEEE/ASME Transactions on Mechatronics, vol. 18, no. 1, pp. 273-284, 2011.
[9] D. Stoianovici et al., "MR safe robot, FDA clearance, safety and feasibility of prostate biopsy clinical trial," IEEE/ASME Transactions on Mechatronics, vol. 22, no. 1, pp. 115-126, 2016.
[10] H. Su et al., "Piezoelectrically actuated robotic system for MRI-guided prostate percutaneous therapy," IEEE/ASME transactions on mechatronics, vol. 20, no. 4, pp. 1920-1932, 2014.
[11] Y. Zhang, B. Li, and L. Yuan, "Study on the Control Method and Optimization Experiment of Prostate Soft Tissue Puncture," IEEE Access, vol. 8, pp. 218621-218643, 2020.
[12] N. Hungr, I. Bricault, P. Cinquin, and C. Fouard, "Design and Validation of a CT- and MRI-Guided Robot for Percutaneous Needle Procedures," IEEE Transactions on Robotics, vol. 32, no. 4, pp. 973-987, 2016.
[13] N. A. Patel, J. Yan, D. Levi, R. Monfaredi, K. Cleary, and I. Iordachita, "Body-Mounted Robot for Image-Guided Percutaneous Interventions: Mechanical Design and Preliminary Accuracy Evaluation," in 2018 IEEE/RSJ International Conference on Intelligent Robots and Systems (IROS), 2018, pp. 1443-1448.
[14] S. Sharma, J. H. Park, J. P. Amadio, M. Khadem, and F. Alambeigi, "A Novel Concentric Tube Steerable Drilling Robot for Minimally Invasive Treatment of Spinal Tumors Using Cavity and U-shape Drilling Techniques," in 2023 IEEE International Conference on Robotics and Automation (ICRA), 2023, pp. 4710-4716.
[15] H. Li, Y. Wang, Y. Li, and J. Zhang, "A novel manipulator with needle insertion forces feedback for robotassisted lumbar puncture," The International Journal of Medical Robotics and Computer Assisted Surgery, vol. 17, no. 2, p. e2226, 2021.
[16] S. Okamoto et al., "Needle artifact characteristics and insertion accuracy using a 1.2T open MRI scanner: A phantom study," Diagnostic and Interventional Imaging, vol. 102, no. 6, pp. 363-370, 2021/06/01/ 2021.
[17] M. F. Khan et al., "Accuracy of biopsy needle navigation using the Medarpa systemcomputed tomography reality superimposed on the site of intervention," European Radiology, vol. 15, no. 11, pp. 2366-2374, 2005/11/01 2005.
[18] H. Su et al., "State of the art and future opportunities in MRI-guided robot-assisted surgery and interventions," Proceedings of the IEEE, vol. 110, no. 7, pp. 968-992, 2022.
[19] M. Ho, A. B. McMillan, J. M. Simard, R. Gullapalli, and J. P. Desai, "Toward a meso-scale SMA-actuated MRI-compatible neurosurgical robot," IEEE transactions on robotics, vol. 28, no. 1, pp. 213-222, 2011.
[20] D. Von Langsdorff, P. Paquis, and D. Fontaine, "In vivo measurement of the frame-based application accuracy of the Neuromate neurosurgical robot," Journal of neurosurgery, vol. 122, no. 1, pp. 191-194, 2015.
[21] A. De Benedictis et al., "Robot-assisted procedures in pediatric neurosurgery," Neurosurgical focus, vol. 42, no. 5, p. E7, 2017.
[22] C. Batailler, D. Hannouche, F. Benazzo, and S. Parratte, "Concepts and techniques of a new robotically assisted technique for total knee arthroplasty: the ROSA knee system," Archives of Orthopaedic and Trauma Surgery, vol. 141, no. 12, pp. 2049-2058, 2021.
[23] L. Liu et al., "Frameless ROSA robot-assisted lead implantation for deep brain stimulation: technique and accuracy," Operative Neurosurgery, vol. 19, no. 1, pp. 57-64, 2020.
[24] F. J. Siepel, B. Maris, M. K. Welleweerd, V. Groenhuis, P. Fiorini, and S. Stramigioli, "Needle and Biopsy Robots: a Review," Current Robotics Reports, vol. 2, no. 1, pp. 73-84, 2021/03/01 2021.
[25] B. Maurin, B. Bayle, J. Gangloff, P. Zanne, M. de Mathelin, and O. Piccin, "A robotized positioning platform guided by computed tomography: Practical issues and evaluation," in Proceedings 2006 IEEE International Conference on Robotics and Automation, 2006. ICRA 2006., 2006: IEEE, pp. 251-256.
[26] N. Plitea, A. Szilaghyi, and D. Pisla, "Kinematic analysis of a new 5-DOF modular parallel robot for brachytherapy," Robotics and Computer-Integrated Manufacturing, vol. 31, pp. 70-80, 2015/02/01/ 2015.
[27] A. Salimi, A. Ramezanifar, J. Mohammadpour, K. Grigoriadis, and N. Tsekos, "ROBOCATH: a patient-mounted parallel robot to position and orient surgical catheters," in Dynamic systems and control conference, 2012, vol. 45318: American Society of Mechanical Engineers, pp. 471-480.
[28] B. Meiklejohn, "The effect of rotation of an epidural needle: an in vitro study," Anaesthesia, vol. 42, no. 11, pp. 1180-1182, 1987.
[29] M. Meltsner, N. Ferrier, and B. Thomadsen, "Observations on rotating needle insertions using a brachytherapy robot," Physics in Medicine and Biology, vol. 52, no. 19, p. 6027, 2007.
[30] R. Mieling et al., "Collaborative Robotic Biopsy with Trajectory Guidance and Needle Tip Force Feedback," arXiv preprint arXiv:2306.07129, 2023.
[31] L. Sheng and W. Li, "Optimization design by genetic algorithm controller for trajectory control of a 3-RRR parallel robot," Algorithms, vol. 11, no. 1, p. 7, 2018.
[32] S. Kock and W. Schumacher, "A parallel xy manipulator with actuation redundancy for high-speed and active-stiffness applications," in Proceedings. 1998 IEEE International Conference on Robotics and Automation (Cat. No. 98CH36146), 1998, vol. 3: IEEE, pp. 2295-2300.
[33] Z. Zhang, L. Wang, and Z. Shao, "Improving the kinematic performance of a planar 3-RRR parallel manipulator through actuation mode conversion," Mechanism and Machine Theory, vol. 130, pp. 86-108, 2018/12/01/ 2018.
[34] C. M. Doherty and R. B. Forbes, "Diagnostic lumbar puncture," The Ulster medical journal, vol. 83, no. 2, p. 93, 2014.
[35] M. S. Ellenby, K. Tegtmeyer, S. Lai, and D. A. Braner, "Lumbar puncture," New England Journal of Medicine, vol. 355, no. 13, p. e12, 2006.